http://dx.doi.org/10.5935/0103-5053.20140209

J. Braz. Chem. Soc., Vol. 26, No. 1, 22-31, 2015.
Printed in Brazil - ©2015 Sociedade Brasileira de Química
0103 - 5053 $6.00+0.00

Article

Cu and Ni Catalysts Supported on γ-Al_2O_3 and SiO_2 Assessed in Glycerol Steam Reforming Reaction

Vivian V. Thyssen, Thaisa A. Maia and Elisabete M. Assaf*

Instituto de Química de São Carlos, Universidade de São Paulo,
Av. Trabalhador Sãocarlense 400, 13560-970 São Carlos-SP, Brazil

Catalisadores de Cu e Ni suportados em γ-Al_2O_3 e SiO_2 comerciais foram estudados frente a reforma a vapor de glicerol. Os catalisadores foram preparados pelo método da impregnação e caracterizados por espectrometria de emissão atômica por plasma acoplado indutivamente, fisissorção de nitrogênio, redução a temperatura programada com H_2 e difração de raios X. A caracterização mostrou a presença de espécies com diferentes interações com os suportes: CuO, NiO e $NiAl_2O_4$. Os testes catalíticos foram realizados a 600 °C e, para o catalisador que apresentou o melhor desempenho, foram realizadas reações a 500 °C e a 700 °C. Os testes mostraram que a presença de $NiAl_2O_4$ desfavorece a deposição de carbono, provavelmente devido à maior dispersão do Ni na superfície do catalisador. Observou-se também que o catalisador NiSi foi o que apresentou a maior atividade para a formação de H_2, porém este apresentou a maior deposição de carbono ao longo da reação.

Cu and Ni catalysts supported on commercial γ-Al_2O_3 and SiO_2 were tested in the glycerol steam reforming. The catalysts were prepared by the impregnation method and characterized by inductively-coupled plasma atomic emission spectrometry, nitrogen physisorption, temperature programmed reduction with H_2 and X-ray diffraction. The characterization indicated several catalytic species in the samples interacting differently with the supports: NiO, CuO and $NiAl_2O_4$. The catalytic tests were performed at 600 °C, and the best catalyst was also tested at 500 °C and 700 °C. The results showed that the presence of $NiAl_2O_4$ did not favor the deposition of carbon during the reaction, probably due to the greater dispersion of Ni on the catalyst surface. It was also observed that, although NiSi was the most active catalyst for H_2 production, it also showed the highest carbon deposit during the reaction.

Keywords: nickel, copper, catalysts, glycerol steam reforming

Introduction

Most of the world's energy demand is supplied by fossil fuel burning. Besides subjecting countries to economic instability due to price fluctuations, these resources generate waste products that seriously endanger the environment, for example by global warming. Moreover, it is also known that one day these resources will be exhausted. Thus, alternative, clean and sustainable energy sources are vitally important.

One such alternative source of energy that stands out is H_2, which can be produced from renewable raw material and whose combustion in fuel cells involves little waste and practically no pollution. H_2 can be produced by steam reforming of hydrocarbons and alcohols, such as methane, naphtha, methanol, ethanol and glycerol.[1]

Glycerol is produced as a byproduct in the transesterification reaction used to make biodiesel (equation 1), which is increasingly used as fuel, and the increase in its production results in a large supply of glycerol on the market. One possible way of using this excess glycerol is in the production of H_2 by glycerol steam reforming reaction (GSR), given that, from 1 mol of glycerol, up to 7 mol of H_2 can be produced (equation 2).[1]

$$C_3H_5(OOC)_3(R_n)_3 + 3R'OH \leftrightarrows 3R_nCOOR' + C_3H_5(OH)_3 \quad (1)$$

$$C_3H_5(OH)_3 + 3H_2O \leftrightarrows 3CO_2 + 7H_2 \quad \Delta H_{f25\,^\circ C} = +123.00\ kJ\ mol^{-1} \quad (2)$$

*e-mail: eassaf@iqsc.usp.br

Buffoni *et al.*[2] observed that the conversion of glycerol into gaseous products depends greatly on temperature, with a minimum temperature of 550 °C to achieve H_2 selectivity.

According to Adhikari *et al.*,[1] the conversion of glycerol into H_2 and CO_2 involves preferential C–C bond cleavage as opposed to the breaking of C–O bonds.

It is well established that catalysts with a noble metal in their compositions have excellent properties in various reactions.[3] However, these catalysts are expensive and highly susceptible to deactivation by poisons such as sulfur. Thus, there is a need to develop catalysts that are specifically suited to each purpose. On account of their low cost and good activity, supported Cu and Ni systems are good alternatives to noble metals.

Carrero *et al.*[4] studied Cu and Ni supported systems and chose Ni as one of the active metals for their catalysts, owing to its good activity in the steam reforming processes.

Researchers suggest that Ni catalysts favor the C–C cleavage of the alcohols, leading to CH_4, CO and H_2 formation, but these catalysts are also known to favor the deposition of carbon, which may impair the performance of the catalyst.[5-7] CuNi bimetallic catalysts have been studied, in order to avoid deactivation by carbon formation, due to the ability of Cu to inhibit such formation.[4]

γ-alumina (γ-Al_2O_3) and silica (SiO_2) are widely used as supports, owing to their high specific areas, which provide a greater contact area and possibly a higher number of active sites for the desired reactions to occur.

Therefore, considering the need to seek new energy sources and knowing the benefits of using H_2, this article focuses on the study of Cu, Ni and CuNi catalysts supported on commercial γ-Al_2O_3 and on SiO_2, applied to the generation of H_2 by the steam reforming of glycerol.

Experimental

Preparation

The catalysts were prepared by the wet impregnation method, with mass contents of 10% Cu and 10% Ni for monometallic catalysts and 5% Cu plus 5% Ni for bimetallic catalysts, supported on the commercial γ-Al_2O_3 and SiO_2.

Commercial SiO_2 (Degussa, Aerosil 200) and γ-Al_2O_3 (Alfa-Aesar) supports were treated at 600 °C for 2 h under a flow of synthetic air, for thermal stabilization and surface water removal. The supports were impregnated with the metals wetting them with aqueous solutions of $Cu(NO_3)_2.3H_2O$ and $Ni(NO_3)_2.6H_2O$, the impregnation of the bimetallic catalysts being performed simultaneously with the two metals; the excess water was removed by rotary evaporation at 80 °C for 6 h and the samples were dried at 80 °C for 12 h. The catalytic precursor oxides were then prepared by calcination for 3 h at 600 °C, under synthetic air flowing at 30 mL min^{-1}. The samples obtained were: 10% Cu/γ-Al_2O_3 (CuAl), 10% Ni/γ-Al_2O_3 (NiAl), 5% Cu 5% Ni/γ-Al_2O_3 (CuNiAl); 10% Cu/SiO_2 (CuSi), 10% Ni/SiO_2 (NiSi) and 5% Cu 5% Ni/SiO_2 (CuNiSi).

Characterization

In order to measure the metal content of each sample, it was analyzed by atomic emission spectrometry of inductively-coupled plasma (ICP), with a Perkin Elmer ICP Optima 3000 DV. Ni and Cu standards were used to determine the calibration curve from which the concentrations of the metals in the catalysts were read.

The nitrogen physisorption (BET method) was used to determine the specific area of the catalysts, employing a Quantachrome Nova 1000e device.

Temperature-programmed reduction with H_2 (TPR-H_2) was carried out on the samples, to study the reduction behavior of the oxide phases and, consequently, to monitor the degree of reduction and the interactions of the metal phases with the support. The TPR-H_2 analyses were carried out in an Analytical Multipurpose System (AMPS3), the catalysts being reduced in a fixed-bed quartz reactor with 1.96% of H_2/Ar (30 mL min^{-1}), subject to a 10 °C min^{-1} heating ramp from 25 °C to 1000 °C.

The catalysts were characterized by X-ray diffraction (XRD) to identify the crystalline phases. The XRD analysis was performed on a Rigaku Multiflex diffractometer, with Cu-Kα radiation. The Bragg angle was scanned at 2° min^{-1}, between 5° and 80° (2θ).

XRD patterns were also recorded *in situ*, under activation conditions, at the XPD-10B beamline of the LNLS synchrotron radiation facility (Campinas, Brazil). The measurements were made in the reflection mode, in a 2θ interval from 30° to 75°, with radiation of λ = 1.54996 Å, calibrated with a Si (1 1 1) monochromator. The oxidized samples were heated in flowing H_2 flow (30 mL min^{-1}), under a ramp of 10 °C min^{-1} from 25 °C to the reduction temperature, and held at that temperature for 1 h, when a diffraction pattern was collected and the average size of the Ni metal crystallites on the catalysts was calculated from Scherrer's equation (3).

$$L = (K.\lambda)/(\beta.\cos\theta) \quad (3)$$

where L is the average width of the crystallite (nm), K is Scherrer's constant (ca. 0.9), λ is the wavelength of incident radiation (nm), β is the half-height width of the most intense peak for the crystalline species (radians) and θ is half the

Bragg angle of that peak (°).

Both the fresh and used catalysts were analyzed by scanning electron microscopy (SEM) to assess the carbon formed on the catalysts. These analyses were performed on a LEO-440 scanning electron microscope equipped with an Oxford detector.

Thermogravimetric analysis (TGA) was performed to measure the weight loss on the used catalysts too, the analyses were performed with TGA/DSC1 supplied by Mettler Toledo.

Catalytic tests

The catalysts were activated (reduced) at various temperatures, which depended on the TPR-H_2 profiles of each sample (NiAl and CuNiAl at 800 °C; CuAl, NiSi and CuNiSi at 500 °C), for 1 h under flowing H_2. The glycerol steam reforming reactions were performed in a tubular quartz reactor with a water:glycerol molar ratio of 3:1, at a flow rate of 2.5 mL h^{-1}, produced with a high precision pump. For each reaction, 150 mg of fresh catalyst was used. The tests were performed at 600 °C for 4 h. The catalyst with better performance was also tested at 500 °C and 700 °C.

The gaseous products were analyzed downstream with an in-line gas chromatograph (GC) (VARIAN GC-3800) with two columns in parallel, each with a thermal conductivity detector (TCD) at the outlet. The columns were packed with Porapak-N and 13X Molecular Sieve, operating between 40 and 80 °C, with He and N_2, respectively, as carrier gas, flowing at 10 mL min^{-1}. The liquid products condensed at the reaction outlet were analyzed with a gas chromatograph (Shimadzu), with H_2 as carrier gas and an HP5 capillary column, operating between 35 and 250 °C. During preparation of the liquid products for GC analysis, the solution was kept at a temperature below 10 °C, to avoid product evaporation.

The glycerol conversion to gaseous products was calculated from equation 4.[2]

$$X_{Glycerol} = \left[\frac{\text{C mol in gas products}}{3 \times \text{glycerol mol in feed}} \right] \times 100 \quad (4)$$

Results and Discussion

Characterization

Table 1 shows the results of the metal content analysis of the catalysts, obtained by ICP, and the specific areas (BET method) of the supports and catalysts. The experiment values for metal content were close to the nominal content, indicating that the preparation method was adequate. Small real differences in the values arise from the handling of the reactants during preparation.

Table 1. Metal contents in the catalysts and specific areas of the catalysts and supports

Sample	Metal content / mass %				Specific area / (m^2 g^{-1})
	Nominal value		Real value		
	Cu	Ni	Cu	Ni	
γ-Al_2O_3	–	–	–	–	220
CuAl	10.0	–	9.1 ± 1.2	–	168
NiAl	–	10.0	–	8.1 ± 0.6	184
CuNiAl	5.0	5.0	4.8 ± 0.3	4.9 ± 0.3	171
SiO_2	–	–	–	–	251
CuSi	10.0	–	8.3 ± 0.8	–	178
NiSi	–	10.0	–	8.8 ± 1.1	172
CuNiSi	5.0	5.0	5.3 ± 0.4	4.8 ± 0.2	158

These results show that there was a decrease in the original support area when metal impregnation was performed. This fact can be explained by assuming that, the Ni and Cu in calcined samples are in the oxide form of NiO and CuO, and these phases do not enlarge the surface area when the support already has a very high surface area, and, reduction in the specific area could result from either a partial obstruction of the pores on the support by the metal oxide or possible agglomeration of the metal on the surface.[8]

Figure 1a shows the results of the TPR analysis of the catalysts with the metals supported on γ-Al_2O_3.

The TPR profile of the NiAl catalyst shows a large peak at 856 °C for reduction of the stoichiometric nickel aluminate species ($NiAl_2O_4$) and a low peak at 256 °C, which can be attributed to the reduction of NiO species that interact weakly with the support. In this catalyst, almost all the Ni is in stoichiometric nickel aluminate.

The literature usually reports the existence of four different species of nickel oxides: the first is reducible in the temperature range 250 °C to 350 °C and appears in the form of segregated crystallites that exhibit a very weak interaction with the support; a second species, reducible in the range 350 °C to 500 °C, consists of NiO in close contact with the support; that reduced in the range 500 °C to 750 °C consists of phases of non-stoichiometric nickel aluminate (NiO-Al_2O_3) and that reduced above 750 °C has the structure of stoichiometric nickel aluminate ($NiAl_2O_4$). Species with stronger interaction with the support show a higher temperature of reduction and are harder to reduce.[9-13]

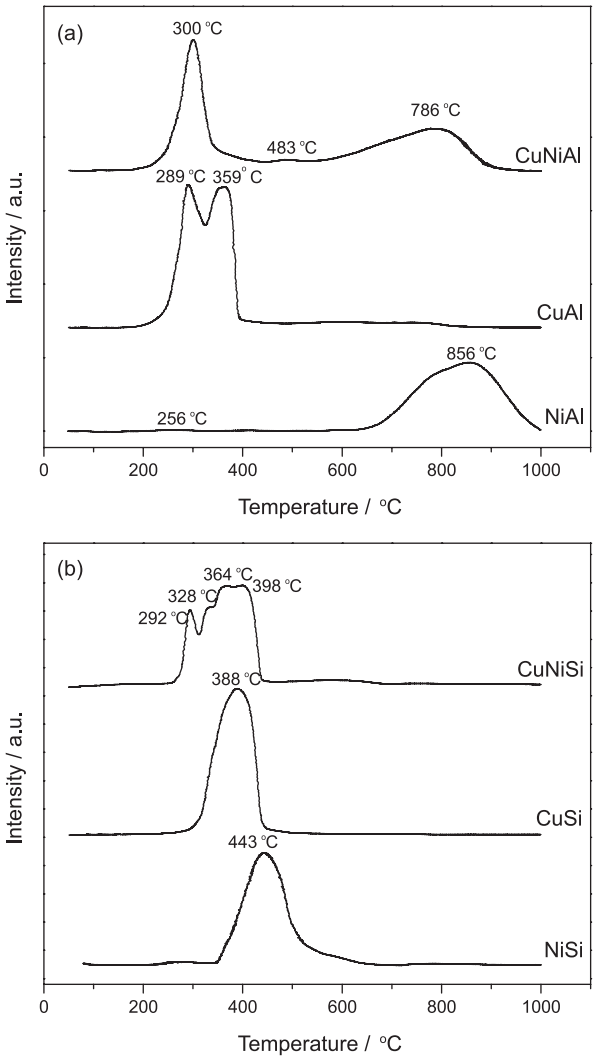

Figure 1. TPR profiles of catalysts supported on (a) γ-Al_2O_3 and (b) SiO_2.

The TPR of the CuAl sample shows two peaks, the first at 289 °C and the second at 359 °C. These peaks can be attributed to the reduction of copper oxide ($Cu^{2+} \rightarrow Cu^0$). The first peak refers to the more dispersed CuO species and the second to CuO crystallites.[9-16]

The CuNiAl catalyst TPR profile shows peaks at 300 °C, 483 °C and 786 °C. According to the literature,[16,17] the first peak refers to the reduction of highly-dispersed copper oxide. There is only one copper oxide reduction peak, which may be due to the presence of nickel species that are reduced at the same temperature, hiding the two reduction peaks of the copper oxide species. The second peak refers to the reduction of NiO species interacting with the support and the third to the reduction of stoichiometric nickel aluminate.[9]

According to Carrero *et al.*,[4] copper has the property of decreasing the reduction temperature of another metal on the support due to synergistic interaction between the metal oxide phases.[18] Thus, the decrease in the temperature of reduction of the $NiAl_2O_4$ species in the bimetallic catalyst can be explained (Figure 1a, 856 °C to 786 °C).

In the TPR of the sample of CuSi (Figure 1b), a peak at 388 °C is observed. This peak can be attributed to the reduction of the copper oxide phase ($Cu^{2+} \rightarrow Cu^0$).[16,19]

The TPR profile of the catalyst NiSi shows a peak at 443 °C, referring to the reduction of Ni^{2+} in the NiO species interacting with the support.[3] Nickel silicates were not detected, as these species would show reduction peaks at a higher temperature.[13] The presence of Ni^{3+} in the sample can be discarded, owing to the absence of a reduction peak at 200 °C.[3,13]

In the TPR of CuNiSi, peaks are observed at 292 °C, 328 °C, 364 °C and 398 °C. The first two peaks can be attributed to the reduction of the CuO species. The first peak refers to the more dispersed CuO species and the second to species in CuO crystallites, which have a higher reduction temperature,[16,19] as already mentioned. The peak at 364 °C can be attributed to NiO species that interact weakly with the support and appear in the form of segregated crystallites, whereas the peak at 398 °C refers to the NiO species that have greater contact with the support but do not form silicates.[13,18] A decrease is observed in the reduction temperature of NiO species in the bimetallic catalyst, compared to the NiSi monometallic catalyst, due to the synergistic interaction between the CuO and NiO phases.[18]

Table 2 shows the H_2 consumption during the reduction of NiO, $NiAl_2O_4$ and CuO and the degree of reduction of the catalytic metals.[14]

Table 2. H_2 consumption by and degree of reduction of oxide phases

Catalyst	H_2 consumption / $\times 10^5$ mol			Reduction / %	
	CuO	NiO	$NiAl_2O_4$	Cu	Ni
CuAl	14.0	–	–	89	–
NiAl	–	–	12.4	–	73
CuNiAl	8.5	2.2	4.2	100	75
Catalyst	H_2 consumption / $\times 10^5$ mol			Reduction / %	
	CuO		NiO	Cu	Ni
CuSi	17.1		–	99	–
NiSi	–		16.2	–	95
CuNiSi	6.2		8.5	95	100

It can be seen that SiO_2-supported catalysts showed a higher degree of reduction of the metals than γ-Al_2O_3-supported catalysts. This can be explained by the interaction of metal oxides with the supports. NiO and CuO species supported on SiO_2 interact weakly with the support and are

thus more easily reduced, while the NiO-γ-Al_2O_3 ($NiAl_2O_4$) shows a strong interaction, making the reduction of the metal more difficult.

Figure 2a shows the diffractograms of the γ-Al_2O_3-supported catalysts. The crystalline phases were identified by comparison with JCPDS standards.[20] The low crystallinity of the catalysts is observed by the presence of broad and poorly defined peaks.

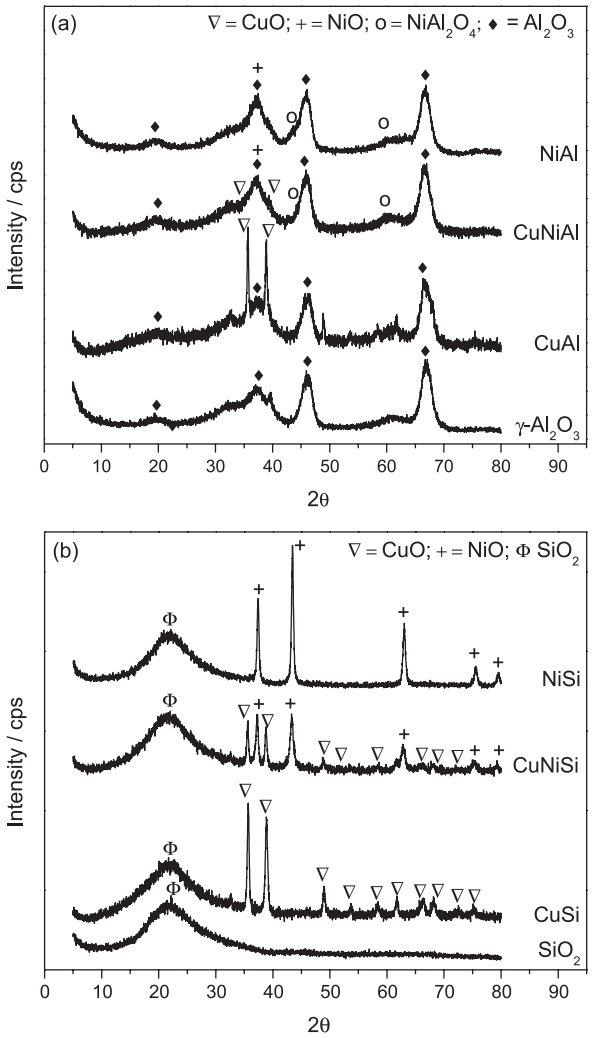

Figure 2. XRD patterns of catalysts supported (a) on γ-Al_2O_3 and (b) on SiO_2.

The peaks appearing at 2θ = 19.6°, 39.7°, 46.1° and 66.5° in all diffraction patterns were attributed to the support structure of γ-Al_2O_3 (JCPDS 82-1468). The signals relating to three other oxide phases were also observed: CuO, NiO and $NiAl_2O_4$. The signals related to the CuO phase were observed at positions 2θ = 35.6° and 38.7°. As for the $NiAl_2O_4$ (JCPDS 10-0339) phase, peaks were observed at 2θ = 46.1° and 59.7°, while for the NiO phase (JCPDS 77-1877) there may be a signal at 37.6°, overlapping a signal related to the support.

Figure 2b shows the diffractograms of the catalysts supported on SiO_2. The peak that appears at 2θ = 22.3°, in all the diffractograms, was attributed to the support structure of SiO_2 (JCPDS 84-0384). Signals referring to two other oxide species were also observed: NiO and CuO. Those related to the NiO phase (JCPDS 77-1877) were observed at 2θ = 37.5°, 43.5°, 63.0°, 75.5° and 79.5° and those related to the CuO copper phase (JCPDS 80-1917) were observed at 2θ = 35.6°, 39.0°, 48.7°, 61.8°, 65.5° and 66.4°.

Figure 3 presents the *in situ* XRD patterns of NiAl and NiSi monometallic catalysts at room temperature and at reduction (activation) temperatures (850 °C and 450 °C, respectively). It may be noted that the peaks previously observed at 2θ = 37°, 43° and 75°, related to NiO species, disappear on reduction and peaks for metallic Ni^0 appear at 2θ = 44°, 52° and 76°.[20] The appearance of the Ni^0 peaks is an evidence of the reduction of NiO species in the catalysts.

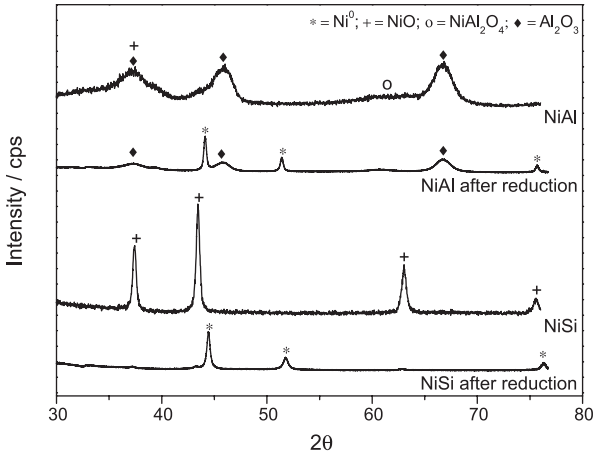

Figure 3. *In situ* XRD for NiAl and NiSi catalysts.

The crystallite size of Ni^0 was estimated by Scherrer's equation (equation 3), and it was found that NiSi (0.4 nm) > NiAl (0.2 nm). The smaller size of Ni^0 crystallites in the NiAl catalyst suggests a greater dispersion of the nickel phase on the γ-Al_2O_3 support. In order to avoid the formation of carbon, according to Chen *et al.*,[21] small Ni crystallites are highly desirable and the crystallite size of metallic Ni is a key factor for the formation of carbon.

Catalytic tests (glycerol steam reforming)

Considering the steam reforming reaction of glycerol (equation 2), with a water:glycerol molar ratio of 3:1, the reaction could, in theory, reach a maximum selectivity of 70% formation of H_2 and 30% of CO_2. However, the presence of CH_4, CO, and in some cases, C_2H_4, as secondary gas products and a number of liquid products, such as acetic acid and ethanol, indicates the occurrence of side reactions.

The results presented in Figure 4 and Table 3 were obtained with the monometallic Ni catalysts and bimetallic catalysts, which were active and stable during the reactions at 600 °C. The monometallic Cu catalysts supported on γ-Al_2O_3 and on SiO_2 were not active for the steam reforming of glycerol under these experimental conditions.

Our results showed that the Cu activity in the steam reforming of glycerol is very low, the reaction being very slow. In the reactions on the monometallic catalysts of Cu, an insignificant H_2 selectivity and a very low glycerol conversion were observed.

Figure 4 shows the evolution of reaction over time on stream to the catalysts. It can be seen that the formation of all products remained constant throughout the reaction at 600 °C.

Table 3 shows the conversion of glycerol (gaseous products),[2] the formation of gaseous products and carbon formation on the Ni monometallic catalysts and CuNi bimetallic catalysts.

It was observed that NiSi was the most active catalyst for H_2 production. However, at the same time, it was the catalyst that produced the greatest carbon deposit during the catalytic test, which is deleterious to the process.

The great CO_2 formation, compared to the CO formation, in the reaction can be explained by the occurrence of the water-gas shift reaction (equation 5).

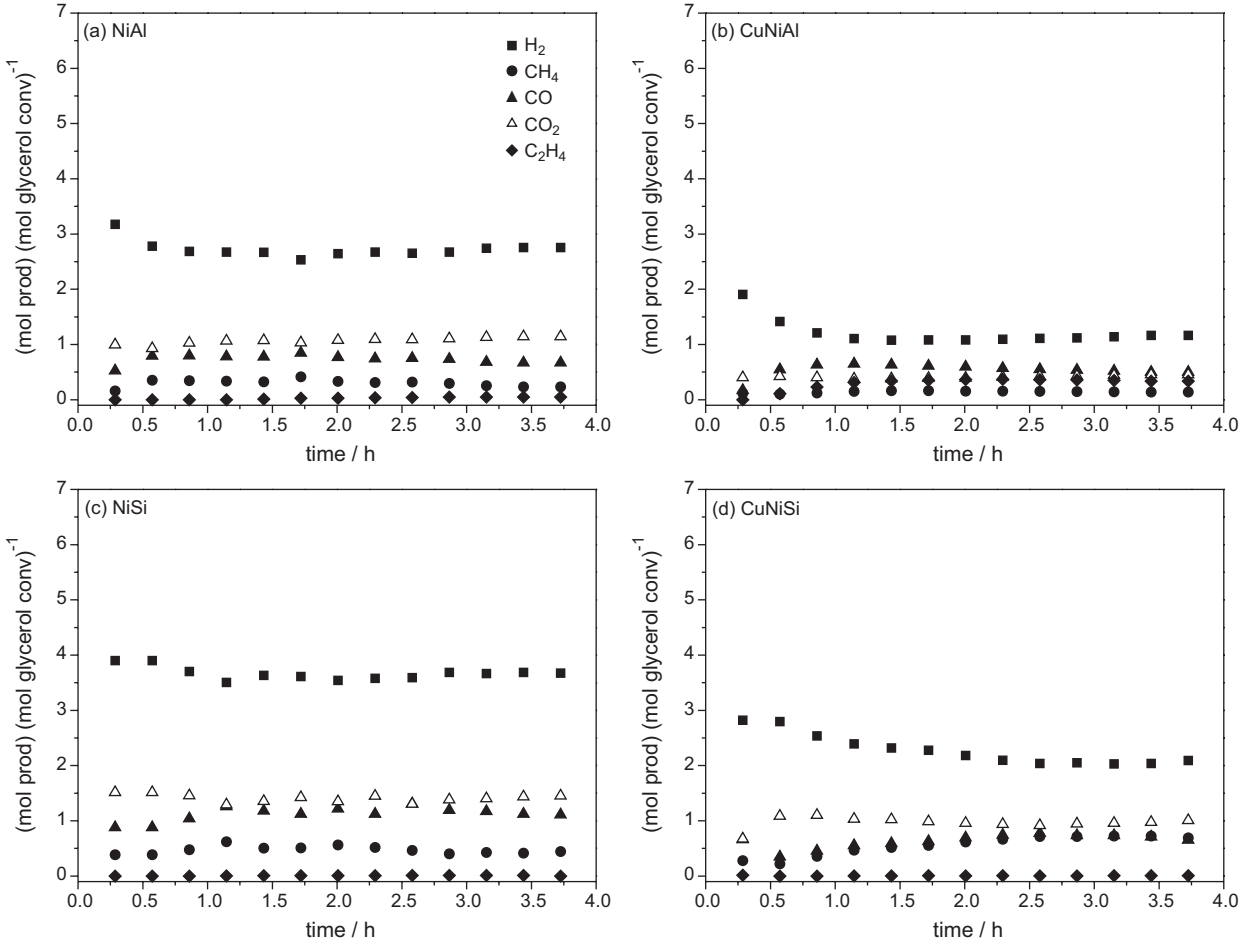

Figure 4. Gas products of catalytic tests of GSR on the catalyst (a) NiAl, (b) CuNiAl, (c) NiSi and (d) CuNiSi, at 600 °C.

Table 3. Conversion (gaseous products), gaseous products/(mol prod).(mol glycerol in feed)$^{-1}$ and carbon formed during GSR/(mmol C prod).[(mol glycerol conv).h]$^{-1}$

Catalyst	Conversion / %	H_2	CH_4	CO	CO_2	C_2H_4	Carbon
				T = 600 °C			
NiAl	69	2.7	0.2	0.3	0.5	–	0.4
CuNiAl	59	1.1	0.1	0.2	0.2	0.4	1.6
NiSi	72	3.7	0.3	0.5	0.7	–	2.2
CuNiSi	64	2.4	0.3	0.3	0.5	–	1.7

Fierro *et al.*[22] explain the occurrence of this reaction by its thermodynamic equilibrium. CO can be produced by the CH_4 steam reforming reaction (equation 6) and by glycerol direct decomposition (equation 7); thence, the equilibrium of the water-gas shift reaction can be shifted to the right, favoring an increase in CO_2 selectivity.

$$CO + H_2O \leftrightarrows CO_2 + H_2 \quad \Delta H_{f25\,°C} = -41.99 \text{ kJ mol}^{-1} \quad (5)$$
$$CH_4 + H_2O \leftrightarrows 3H_2 + CO \quad \Delta H_{f25\,°C} = +205.4 \text{ kJ mol}^{-1} \quad (6)$$
$$C_3H_5(OH)_3 \leftrightarrows 3CO + 4H_2 \quad \Delta H_{f25\,°C} = +339.6 \text{ kJ mol}^{-1} \quad (7)$$

It can be seen that on SiO_2-supported catalysts, no C_2H_4 was formed during the reaction, while on the γ-Al_2O_3-supported catalysts C_2H_4 appears among the products. The formation of C_2H_4 is attributed to the acid sites in the γ-Al_2O_3 support.[23] It can also be seen that on the catalyst NiAl, the formation of C_2H_4 was lower than on the bimetallic catalyst CuNiAl, owing to a higher Ni content in the monometallic catalyst, which favors C–C cleavage into the products CO_2, CO, CH_4 and H_2.

The lower Ni content in the Ni–Cu catalysts may also explain the decrease in H_2 formation; moreover, the addition of Cu to Ni-based catalysts can interfere with Ni availability on the surface of the material, thus hindering the Ni from cleaving the C–C bond and forming the expected gaseous products.

On the catalyst NiAl, the formation of carbon was lower than on all the other catalysts. The carbon may be formed by disproportionation of CO, leading to the formation of CO_2 and C, in the Boudouard reaction (equation 8). Another possibility is the dissociation of CH_4 (equation 9).

$$2CO \leftrightarrows CO_2 + C \quad \Delta H_{f25\,°C} = -172.6 \text{ kJ mol}^{-1} \quad (8)$$
$$CH_4 \leftrightarrows 2H_2 + C \quad \Delta H_{f25\,°C} = +74.9 \text{ kJ mol}^{-1} \quad (9)$$

The carbon formed during the reaction is expected to be at the metal-support interface, forming a filament and separating the metallic Ni from the support, until the catalyst is deactivated by loss of the active phase, which happens with the breakup of the filament.[24] Thus, Ni, which favors the cleavage of C–C bonds (forming CO, CO_2, CH_4 and H_2), loses this property.

The occurrence of the Boudouard reaction (equation 8) on the Ni catalysts should be considered likely, since the presence of the NiO species, observed in the TPR and XRD tests of the CuNiAl, NiSi and CuNiSi catalysts, favors the diffusion of carbon atoms. This diffusion occurs more readily in the presence of NiO, because this species does not interact strongly with the support, so that carbon atoms are more easily distributed on the interface between the metal and the support. However, in the presence of nickel aluminate, this diffusion is hindered, since this species interacts more strongly with the support.[25]

The nickel aluminate species, as precursors of catalysts, have been presented as the most stable species for nickel reforming reactions, on account of the strong $NiAl_2O_4$ interaction, which favors the dispersion of Ni^0 species after activation and during the catalytic tests, in turn preventing Ni^0 sintering, thereby increasing their resistance to deactivation by carbon formation. The addition of copper to the Ni catalyst led to the formation of nickel species interacting more weakly with the support, which do not benefit the catalytic process. Furthermore, the greater formation of stoichiometric Ni aluminate, identified by XRD and TPR analysis, in the monometallic Ni catalyst supported on alumina, may explain its lower carbon deposition during the reaction. This fact is consistent with the results already presented in the characterization of the catalysts, in which NiAl showed the smaller Ni^0 crystallite size.

The addition of Cu to the NiSi catalyst led to a decrease in carbon formation during the reaction. The literature reports that Ni catalysts promote the formation of carbon, which is deposited between the metal phase and the support surface, as already mentioned, forming a filament that can be broken, thereby causing catalyst deactivation by the loss of the active phase. Cu does not favor the formation of carbon, as it changes the affinity of Ni for CO, not favoring the occurrence of the Boudouard reaction (equation 8).[9]

The difference in the carbon formation between the catalysts supported on γ-Al_2O_3 and on SiO_2 can be explained by the presence of $NiAl_2O_4$, which favors Ni^0 dispersion. According to the TPR results, SiO_2-supported catalysts did not show any kind of Ni interacting strongly with the support.

Electron micrographs of fresh and used NiAl and NiSi catalysts are shown in Figure 5 and it may be noted that the fresh catalysts exhibit different morphologies. After the reaction, on both NiAl and NiSi catalysts, carbon formation is evident, the carbon filament formation being greater on NiSi than on NiAl.

According to Lee and Li,[26] Ni catalysts lead to the formation of filamentous carbon during the reaction. This process leaves the active surface available, but continued filament growth results in fragmentation of the catalyst with loss of active phase.

The TGA profiles for used NiAl and NiSi catalysts samples are shown in Figure 6.

It can be seen that on NiAl catalyst, the carbon mass loss is lower than that on NiSi, which corroborates the theory that the greater dispersion of Ni on NiAl catalyst ($NiAl_2O_4$ formation) difficult the carbon deposition on the

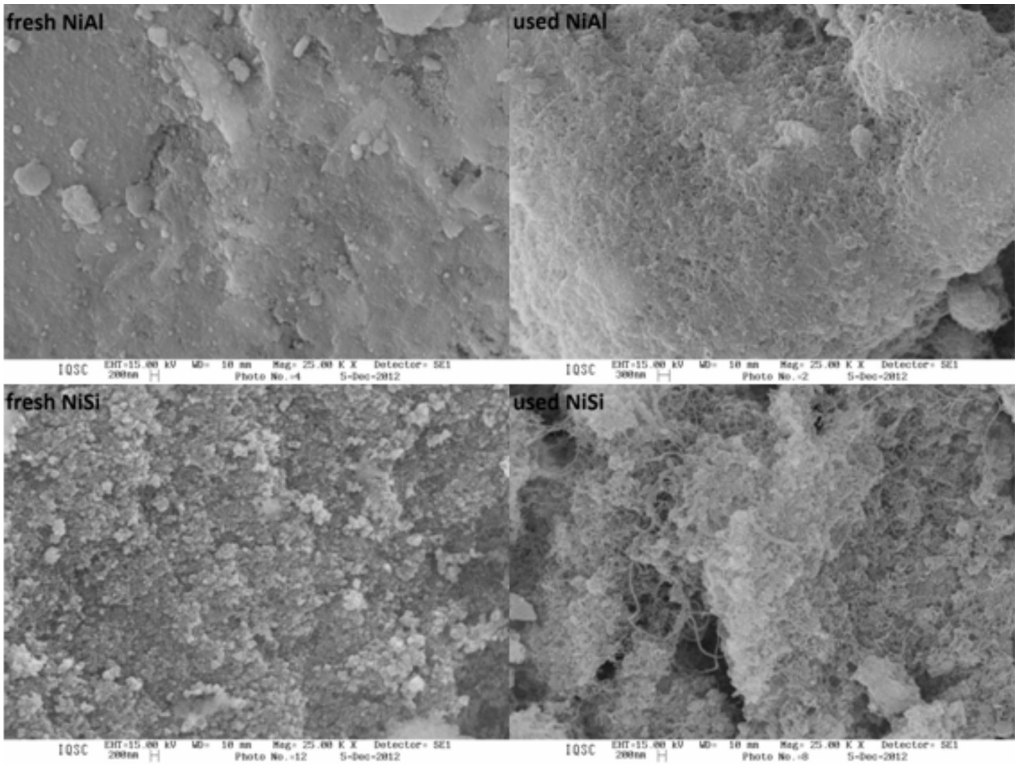

Figure 5. SEM images of fresh and used NiAl and NiSi catalysts.

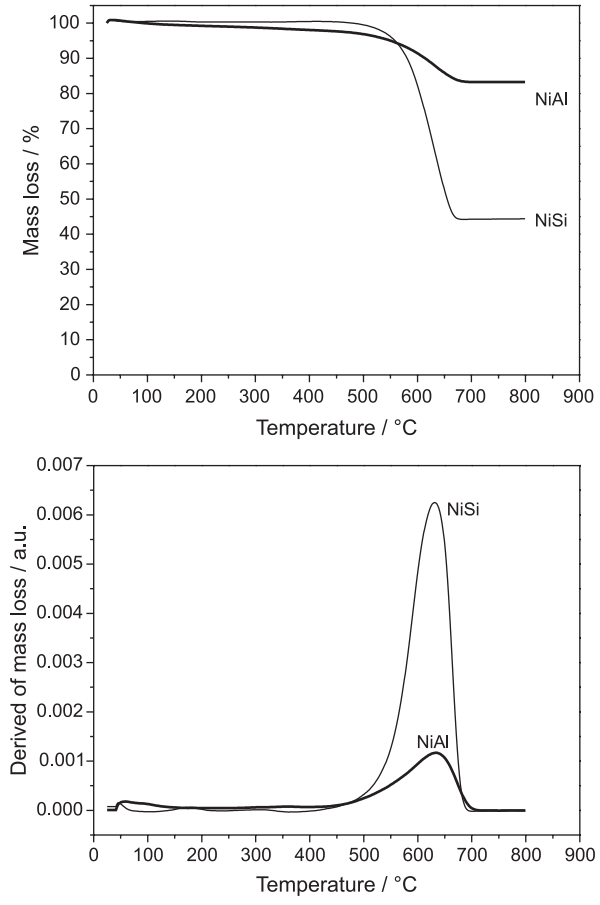

Figure 6. TGA-DSC1 profiles of used NiAl and NiSi catalysts.

catalyst; whereas in the NiSi catalyst, the presence of NiO explains the higher deposition of carbon in these material.

Figure 7 shows the catalytic performance of NiAl at 500 °C and 700 °C, and Table 4 shows the conversion of glycerol (to gaseous products), the formation of gaseous products and carbon on the NiAl catalyst, at the various temperatures.

The observed drop in CH_4 selectivity and the rise in the CO and H_2 selectivity at 700 °C can be explained by the thermodynamic equilibrium of the steam reforming of methane (equation 6), which is favored at the higher temperature. It was also observed that carbon formation decreased with increasing temperature, which can be explained by the inhibition of the Boudouard reaction (equation 8), since this is an exothermic reaction.

The CO_2 formation, at 500 °C and 600 °C (Figure 4) was greater than that of CO, which can be explained by the occurrence of the water-gas shift reaction (equation 5). However, at 700 °C, it can be seen that a reversal in the selectivity of these products occurred significantly more CO being formed than CO_2, which can be explained by the occurrence of the steam reforming of methane (equation 6) and by the direct decomposition of glycerol (equation 7), as well as the reverse water-gas shift reaction, both of which are favored at this temperature.

The reverse water-gas shift reaction can also explain the drop in H_2 yield (6 to 4 mol prod/mol glycerol in feed)

Table 4. Conversion of glycerol (to gaseous products), gaseous products/(mol prod).(mol glycerol in feed)$^{-1}$ and carbon formed during GSR on the catalyst NiAl/(mmol C prod).[(mol glycerol conv).h]$^{-1}$, at 500 °C, 600 °C and 700 °C

Temperature / °C	Conversion / %	H_2	CH_4	CO	CO_2	C_2H_4	Carbon
				NiAl			
500	64	2.1	0.3	0.1	0.4	–	1.1
600	69	2.7	0.2	0.3	0.5	–	0.4
700	75	4.6	0.1	1.0	0.5	0.2	0.2

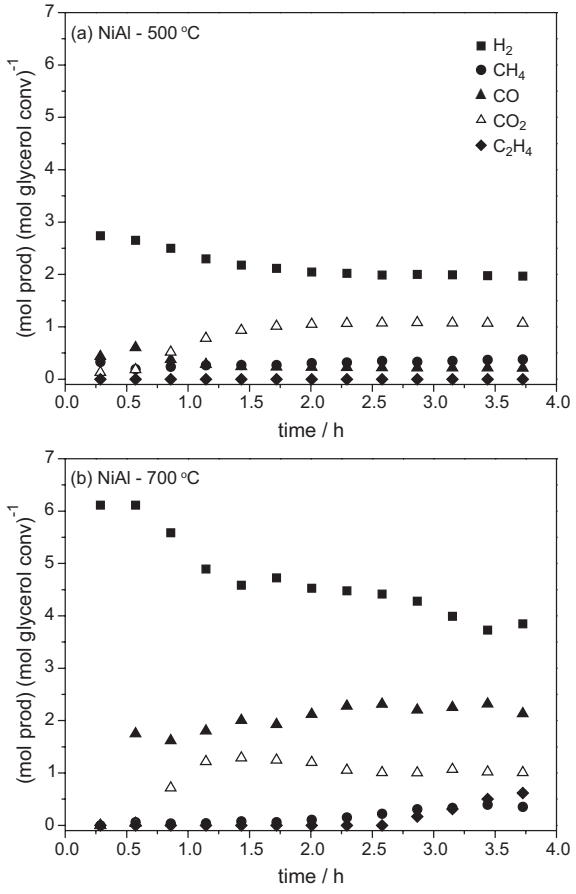

Figure 7. Tests of the catalyst NiAl in the GSR reaction at (a) 500 °C and (b) 700 °C.

during the reaction at 700 °C, at the same time that CO_2 yield decreases, a rise in CO yield is observed.

Besides the gaseous products, the reaction of steam and glycerol also formed liquids under these conditions. The liquids formed during the reaction were identified (not quantified) as a mixture of acetic acid, 1,2,3-butanetrioltrinitrate, diglycerol, 1,2-propanediol, propanal, butanoic acid, pentanoic acid, 2-propanol, ethanol and ethylene glycol.

Conclusions

In the characterization of the catalysts, various kinds of metal-support interaction were observed, the catalysts supported on alumina showing stronger interactions than those supported on silica. These interactions were reflected in the catalytic performance and, from the present results, it was possible to conclude that the formation of nickel-aluminate impeded the deactivation of the catalyst by carbon deposition. The best catalytic performance, with high H_2 selectivity and the lowest carbon formation, was observed on the catalyst NiAl at 700 °C.

References

1. Adhikari, S.; Fernando, S.; Gwaltney, S. R.; To, S. D. F.; Bricka, R. M.; Steele, P. H.; Haryanto, A.; *Int. J. Hydrogen Energy* **2007**, *32*, 2875.
2. Buffoni, I. N.; Pompeo, F.; Santori, G. F.; Nichio, N. N.; *Catal. Commun.* **2009**, *10*, 1656.
3. Kirumakki, S. R.; Shpeizer, B. G.; Sagar, G. V.; Chary, V. R.; Clearfield, A.; *J. Catal.* **2006**, *242*, 319.
4. Carrero, A.; Calles, J. A.; Vizcaíno, A. J.; *Appl. Catal., A* **2007**, *327*, 82.
5. Mariño, F.; Boveri, M.; Baronetti, G.; Laborde, M.; *Int. J. Hydrogen Energy* **2001**, *26*, 665.
6. Mariño, F.; Baronetti, G.; Jobbagy, G.; Laborde, M.; *Appl. Catal., A* **2003**, *238*, 41.
7. Galvita, V. V.; Semin, G. L.; Belyaev, V. D.; Semikolenov, V. A.; Tsiakaras, P.; Sobyanin, V. A.; *Appl. Catal., A* **2001**, *220*, 123.
8. Chica, A.; Sayas, A.; *Catal. Today* **2009**, *146*, 37.
9. Lee, J.; Lee, E.; Joo, O.; Jung, K.; *Appl. Catal., A* **2004**, *269*, 1.
10. Rynkowski, J. M.; Paryjczak, T.; Lenik, M.; *Appl. Catal., A* **1993**, *106,* 73.
11. Lu, Y.; Xue, J.; Yu, C.; Liu, Y.; Shen, S.; *Appl. Catal., A* **1998**, *174*, 121.
12. Dewaele, O.; Froment, G. F.; *J. Catal.* **1999**, *184*, 499.
13. Vos, B.; Poels, E.; Bliek, A.; *J. Catal.* **2001**, *198*, 77.
14. Dong, W. S.; Roh, H. S.; Jun, K. W.; Park, S. E.; Oh, Y. S.; *Appl. Catal., A* **2002**, *226,* 63.
15. Zhang, X.; Liu, J.; Jing, Y.; Xie, Y.; *Appl. Catal., A* **2003**, *240,* 143.
16. Dow, W. P.; Huang, T. J.; *Appl. Catal., A* **1996**, *141*, 17.
17. Dow, W. P.; Wang, Y. P.; Huang, T. J.; *Appl. Catal., A* **2000**, *190*, 25.
18. Burch, R.; Chappell, R. J.; *Appl. Catal.* **1988**, *45*, 131.

19. Chen, L. F.; Guo, P. J.; Qiao, M. H.; Yan, S. R.; Li, H. X.; Shen, W.; Xu, H. L.; Fan, K. N.; *J. Catal.* **2008**, *257*, 172.
20. JCPDS International Centre for Diffraction Data (JCPDS-ICDD 1994), *Joint Committee on Powder Diffraction Standards*; Pensilvânia USA, 1994. CD ROM.
21. Chen, H.; Yu, H.; Peng, F.; Yang, G.; Wang, H.; Yang, J.; Tang, Y.; *Chem. Eng. J. (Loughborough, Engl.)* **2010**, *160*, 333.
22. Fierro, V.; Akdim, O.; Provendier, H.; Mirodatos, C.; *J. Power Sources* **2005**, *145*, 659.
23. Maia, T. A.; Bellido, J. D. A.; Assaf, E. M.; Assaf, J. M.; *Quim Nova* **2007**, *30*, 339.
24. Trimm, D. L.; *Catal. Today* **1999**, *49*, 3.
25. Bradford, M. C. J.; Vannice, M. A.; *Appl. Catal., A* **1996**, *142*, 73.
26. Lee, W. J.; Li, C.; *Carbon* **2008**, *46*, 1208.

Submitted: December 10, 2013
Published online: September 12, 2014

FAPESP has sponsored the publication of this article.